Statistics of Mixing Parameters in the Upper Ocean During JASIN Phase 2

N. S. OAKEY

Department of Fisheries and Oceans, Atlantic Oceanographic Laboratory, Bedford Institute of Oceanography, Dartmouth, Nova Scotia, Canada B2Y 4A2

(Manuscript received 24 September 1984, in final form 13 May 1985)

ABSTRACT

Turbulence levels obtained during the 1978 Joint Air–Sea Interaction experiment (JASIN) have been examined from measurements of both temperature gradient and velocity shear. These measurements, obtained with the vertical profiler OCTUPROBE 2, have been analyzed to compute viscous dissipation rate, ϵ, and dissipation of temperature variance, χ_T. As in a previous study, the dissipation rate increased as the surface energy input parameterized by U_{10}^3 increased. The JASIN study indicated only one-third of the viscous dissipation rate observed in a similar experiment in a region on the Scotian shelf and this difference is discussed. A mixing parameter, Γ, related to the flux Richardson number has been estimated from simultaneous measurements of ϵ and χ_T. The mean value of Γ corresponds to a flux Richardson number of 0.21. Heat flux estimates from temperature microstructure measurements were found to be consistent with other results of the JASIN experiment. The statistical distributions of dissipation, ϵ, mixing parameter, Γ, and other quantities were found to be consistent with lognormality. This result has been used to estimate error limits of mean quantities which may be used as parameters in mixed layer models.

1. Introduction

In the present paper a descriptive picture of turbulent mixing parameters, dissipation of turbulent kinetic energy, ϵ, and dissipation of temperature variance, χ_T, will be presented for phase 2 of the Joint Air–Sea Interaction (1978) experiment (JASIN). The JASIN experiment is summarized by Pollard *et al.* (1983). Velocity and temperature microstructure measurements were made during JASIN using the vertical profiling instrument OCTUPROBE 2 in the Rockall Trough area for the three-week period from 20 August to 8 September 1978 from the ship RRS *Shackleton*. In a previous mixed layer experiment on the Scotian Shelf, Oakey and Elliott (1982) found a strong correlation between the intensity of dissipation, ϵ, and the surface wind forcing at a fixed site. In the discussion to follow it will be shown that the same correlation exists in the JASIN data set. Because measurements were made at different sites, the variability in ϵ resulting from the surface stress and from spatial changes in the large-scale oceanography of the survey area may be difficult to separate. The intensity of velocity microstructure will be compared to the intensity of temperature microstructure to estimate mixing rates.

In the discussion of the microstructure measurements it is useful at this point to review some of the formalism and define some of the quantities that will be used in the description of the data to follow. A simple set of equations that might be used to describe the turbulence in the oceans (Caldwell, 1983) are the turbulent kinetic energy (TKE) equation and the analogous equation for temperature variance. The TKE equation, in the approximate form,

$$\frac{d}{dt}\left(\overline{\frac{1}{2}q^2}\right) = -\overline{u'w'}\frac{\partial U}{\partial z} - \epsilon - g\frac{\overline{\rho'w'}}{\rho} \qquad (1.1)$$

states that the rate of change of mean TKE per unit mass, $\overline{\frac{1}{2}q^2}$, is the sum of three quantities: 1) the rate of production of TKE by Reynolds stress working against the mean shear; 2) the rate of dissipation of TKE per unit mass, ϵ; and 3) the rate of change of potential energy through the buoyancy flux. In this equation, primed variables are fluctuating quantities, unprimed variables are mean quantities, and the equation ignores divergences and redistribution terms from the usual Reynolds decomposition. For isotropic turbulence the dissipation, ϵ, is given by

$$\epsilon = \frac{15}{2}\nu\overline{\left(\frac{\partial u'}{\partial z}\right)^2} \quad [\mathrm{W\ kg^{-1}}] \qquad (1.2)$$

where ν is the kinematic viscosity and the variance of the turbulent shear $(\partial u'/\partial z)^2$ is a measured quantity as described below. The analogous equation for temperature fluctuations is given as

$$\frac{d}{dt}\overline{\left(\frac{1}{2}T'\right)^2} = -\overline{w'T'}\frac{\partial T}{\partial z} - \frac{1}{2}\chi_T \qquad (1.3)$$

which expresses the balance of the time rate of change of temperature variance (TV) being equal to the production of TV by buoyancy flux and the dissipation of TV by molecular diffusion. The dissipation of tem-

perature variance, χ_T, is analogous to ϵ and for isotropy is given by

$$\chi_T = 2D\overline{\nabla T'^2} = 6D\overline{\left(\frac{\partial T'}{\partial z}\right)^2} \quad [°C^2\ s^{-1}] \qquad (1.4)$$

where D is the molecular diffusion constant. The temperature gradient variance $(\partial T'/\partial z)^2$ is a measured quantity described in the next section. If the time rate of change of TV is small, and if we can parameterize the buoyancy flux by a vertical eddy diffusivity, K_T, as follows

$$-\overline{w'T'} = K_T \partial T/\partial z \qquad (1.5)$$

we obtain the familiar Osborn–Cox (1972) relationship. This is

$$K_T = (2 \pm 1)DC_x \quad m^2\ s^{-1} \qquad (1.6)$$

where $C_x = \overline{(\partial T'/\partial z)^2}/(\partial \bar{T}/\partial z)^2$ is the Cox number. The factor (2 ± 1) expresses the isotropy factors which includes the situation from completely layered (1) to isotropic structure (3). In this model, the vertical heat flux becomes

$$Q = -\rho C_p K_T \left(\frac{\partial \bar{T}}{\partial z}\right) \quad [W\ m^{-2}] \qquad (1.7)$$

where C_p is the specific heat and ρ is the density.

If Eq. (1.1) is examined under the assumption that the turbulent kinetic energy level remains constant; expressing the flux Richardson number, R_f, as the ratio of the increase in buoyancy flux to the production of TKE and assuming further that we can parameterize the buoyancy flux using an eddy coefficient as in (1.5)

$$-\overline{w'\rho'} = K_\rho \frac{\partial \rho}{\partial z}, \qquad (1.8)$$

then we can write

$$K_\rho = \frac{R_f}{1 - R_f}\frac{\epsilon}{N^2} = \Gamma \frac{\epsilon}{N^2} \quad [m^2\ s^{-1}]. \qquad (1.9)$$

This has been discussed by Osborn (1980) and Oakey (1982). If eddy coefficients for different scalar variables are the same (Munk, 1966) then K_ρ can be considered equivalent to K_T. Estimating K_T from equation (1.6) and assuming further that $N^2 = g\alpha\partial\bar{T}/\partial z$ one finds that the mixing efficiency, Γ, is given by

$$\Gamma = g\alpha\left(\frac{1}{3} \pm \frac{1}{6}\right)\frac{\chi_T}{\epsilon\partial\bar{T}/\partial z}. \qquad (1.10)$$

Hence by simultaneously measuring the temperature gradient variance and velocity shear variance along with the mean temperature gradient one can estimate Γ.

In the sections to follow a summary of the instrumentation used to measure temperature and velocity microstructure will be given. The ϵ and χ_T data for the JASIN area will be presented as a function of depth and time and the correlation with wind speed examined. It will be shown that ϵ, χ_T and quantities such as Cox number and vertical heat flux are all positively correlated with the surface energy input which is parameterized by the 10-m wind speed, U_{10}^3. The mixing efficiency, Γ, has been calculated and its statistical distribution is consistent with lognormality.

2. Instrumentation

Vertical profiles of microscale velocity and temperature fluctuations were obtained using the instrument OCTUPROBE 2 (OCeanic TUrbulence PROBE). This instrument is described in several papers (Oakey, 1977; Oakey and Elliott, 1982; and Oakey, 1982) and only a brief review will be given here for completeness. OCTUPROBE 2 consists of a cylinder 1.6 m long by 0.15 m diameter containing electronics and a tape recorder. Forward "stings" support a variety of microstructure sensors and preamplifiers. The vehicle is ballasted and drag stabilized to drop vertically, stings and sensors leading, at 0.5–0.7 m s^{-1}. It is recovered and redeployed using a light tether line so that five or six vertical profiles can be obtained to a maximum depth of 100 m during the 25-minute recording limit set by the internal tape recorder. During each vertical profile, temperature gradient microstructure and two perpendicular components of the vertical shear of horizontal microstructure are recorded along with temperature and pressure signals. Temperature microstructure is measured using a platinum thin-film thermometer and horizontal velocity is measured using shear probes, which are described in a number of papers (Siddon, 1971; Osborn and Siddon, 1975; Osborn and Crawford, 1980; Oakey, 1977; Oakey and Elliott, 1982; and Oakey, 1982). A thorough description of the calibration errors and noise correction is given by Oakey (1982).

3. Data analysis

A subset of the data from the JASIN experiment is described by Oakey (1982) and representative profiles of velocity and temperature microstructure are presented in that paper. For a detailed description of the basic analysis and spectral corrections the reader is referred to section 4, "Spectral Computation," in that paper.

The final spectral products are block- and band-averaged corrected power spectra [(physical units)^2/Hz versus frequency] for each 10–15 m of vertical profile for each of the two components of velocity shear and temperature gradient. A noise spectrum was obtained from those sections of the data where the signal was the lowest for each type of sensor. This was substracted from each spectrum. Examples of corrected power spectra of velocity shear and temperature gradient are given in Figs. 4 and 5 of Oakey (1982) for some of the data obtained in JASIN. The variance in velocity shear or temperature gradient is obtained by integrating the area under the power spectrum or the corresponding

variance-conserving spectrum. Dissipation estimates, ϵ, are obtained from Eq. (1.2) using a value of viscosity $\nu = 1.27 \times 10^{-6}$ m^2 s^{-1}. Values of χ_T are obtained from Eq. (1.4) using a value of molecular diffusivity, $D = 1.39 \times 10^{-7}$ m^2 s^{-1}.

The noise level was seldom a problem in determining the velocity shear variance. For temperature gradient, on the other hand, where the cut-off scale is much smaller than for velocity shear, the noise spectrum often limited the variance integration to a scale larger than the cutoff scale. This was particularly true in the mixed layer where the temperature signal was small and the turbulence levels high. A correction to the temperature gradient variance was performed as follows. From the dissipation measurement, ϵ, the Batchelor cutoff wavenumber for the temperature gradient, $k_B = (\epsilon/\nu D^2)^{1/4}$ m^{-1} was computed. As shown by Oakey (1982) the Batchelor (1959) spectrum calculated this way agrees well with the data when the spectrum is well resolved. From the wavenumber at which the variance integral is terminated because of the noise, k_C, and from the value of k_B one can estimate the percentage of the temperature gradient variance measured to the cut-off if the spectrum followed the Batchelor form. The measured value was then corrected accordingly. Typically this correction is less than 10% for $\epsilon < 10^{-8}$ W kg^{-1} and <30% for $\epsilon < 10^{-7}$ W kg^{-1}.

Depth intervals for each of the computed spectra were determined from the OCTUPROBE pressure records. Mean temperature gradients were obtained from the signal recorded from a thermistor and the corresponding depth intervals. Mixed-layer depths were estimated as the first "significant step" in the density profile calculated from the CTD profiles obtained just prior to or just after the microstructure profiles. The total energy dissipated over the mixed layer, ϵ_I, was obtained by summing the values of ϵ weighted by the appropriate depth interval to the mixed layer depth. The data set and computed quantities such as the Cox Number, C_x, and vertical diffusivity, K_z, are discussed below.

4. Velocity and temperature microstructure levels

During the period from 25 August to 8 September, thirty OCTUPROBE stations were occupied using the ship the RRS *Shackleton* in the square delineated by 58°30′N–60°30′N, 9°W–15°W with the majority in the vicinity of 59°N between 12°W and 13°W. These station positions are shown in Fig. 1 identified with the station number. At each station 4–6 vertical microstructure profiles to a depth of 60–80 meters were recorded. The data were analyzed as described previously in vertical segments of 10–15 m and for each segment a value of $\epsilon_u(z)$, $\epsilon_v(z)$, and $\chi_T(z)$ was computed where the subscripts u and v refer to the two measurements of ϵ from the two perpendicular shear probes. These two values are averaged. For each station, the

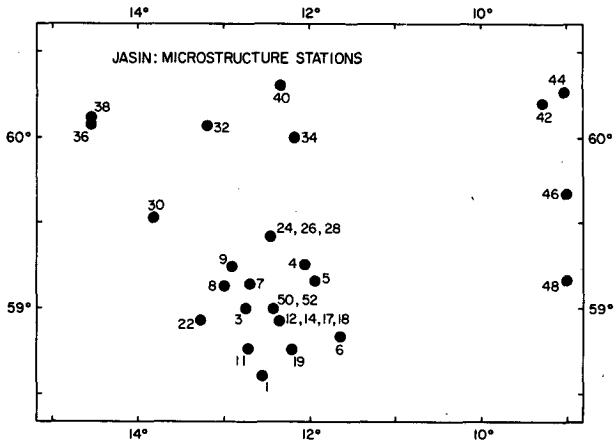

FIG. 1. Positions of microstructure stations in JASIN.

individual 4–6 profiles were analyzed over the same depth intervals. These were averaged to give mean values of $\bar{\epsilon}(z)$ and $\overline{\chi_T(z)}$ over the station period of 25 min. Figure 2 summarizes the data from over 1500 spectra. Each station number is marked below and values of $\bar{\epsilon}(z)$ are recorded in microwatts per cubic meter averaged over the depth intervals delineated by the horizontal tic marks. The numbers range from ≈ 1 μW m^{-3} on Julian day 239 (27 August) to a high of 715 μW m^{-3} on day 247 (4 September). The mixed layer depth is indicated by the curved line. Values of $\bar{\epsilon}(z)$ were integrated to this depth to obtain values of ϵ_I W m^{-2} which are plotted as solid circles in Fig. 2 below the $\bar{\epsilon}(z)$ values. The uppermost value of $\bar{\epsilon}(z)$ was used to estimate the top few meters which were not measured because of the surface wave and ship contamination of the data. The estimates of the surface energy flux in the wind field were obtained from the best estimate of the JASIN hourly 10-m winds, U_{10}, at the *Shackleton*'s position (T. Guymer, personal communication, 1982). The flux has been calculated using the formula

$$E_{\text{wind}} = \rho_a C_{10} U_{10}^3$$

where $\rho_a = 1.2$ kg m^{-3} is the density of the air and $C_{10} = 1.3 \times 10^{-3}$ is the drag coefficient. These values are plotted in Fig. 2 (×) along with ϵ_I. There is a high correlation between the energy flux in the wind field and the dissipation in the mixed layer, particularly after day 246 when the winds were higher.

The values of $\bar{\chi}_T(z)$ are also shown in Fig. 2 in the same manner as the values of $\bar{\epsilon}(z)$. They range from the noise level of 1×10^{-8} °C^2 s^{-1} to values as large as 271×10^{-8} °C^2 s^{-1} on day 248 just below the base of the mixed layer after the winds had freshened over the previous day.

The strong dependence of the mixed layer dissipation rate on the surface energy flux to the mixed layer from the atmospheric boundary layer is shown in Fig. 3. This is compared to the results from a fixed site at

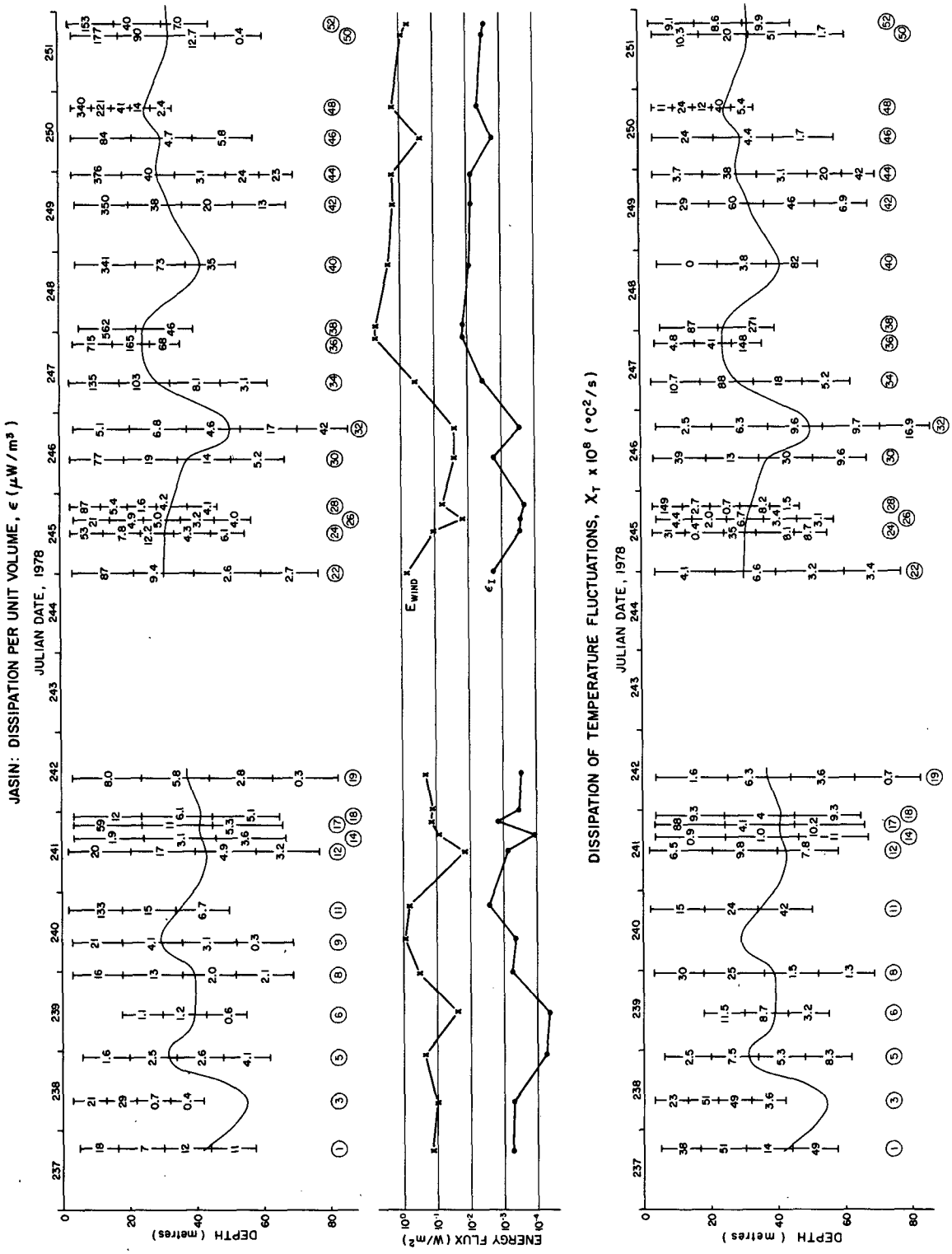

FIG. 2. JASIN summary plot. In the upper and lower panels vertical bars, labeled below by station number, are plotted on the time axis. On each bar, horizontal tic marks delimit the depth intervals over which analyses were performed. Between tic-marks are numbers which are the average dissipation, $\bar{\epsilon}(z)$ (μW m^3) of 4–6 profiles in the upper panel and of temperature fluctuations, χ_T (°C^2 s^{-1}), in the lower panel. The curved line represents the mixed layer depth. The log of the integrated dissipation, ϵ_I (W m^{-2}), and the atmospheric boundary layer energy flux, E_{wind} (W m^{-2}), are plotted in the center panel.

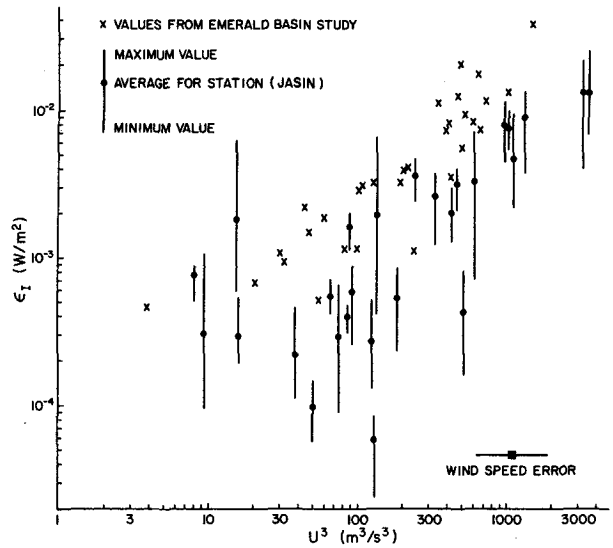

FIG. 3. The dissipation integrated over the mixed layer, ϵ_I (W m^{-2}), is shown for the JASIN experiment (dots) versus the values of U_{10}^3. The vertical bars indicate the largest and smallest of the 4–6 values used to obtain the average. For comparison, the Emerald Basin values (crosses) are shown.

Emerald Basin (Oakey and Elliott, 1982). The JASIN data, ϵ_I, are plotted as closed circles with a vertical bar indicating the largest and smallest value of ϵ_I obtained at each station. Emerald Basin dissipation data are indicated by the symbol $\times$. The notable feature about both sets of data is the strong correlation of ϵ_I to U_{10}^3. However, while the Emerald Basin data indicate that 1.2% of the energy flux across the 10 m level in the atmospheric boundary layer appears as dissipation in the mixed layer, in the JASIN study, this fraction is only about 0.4% or one-third of the value found previously. This difference cannot be explained on the basis of statistical or systematic errors in the determination of ϵ and U_{10}. The maximum systematic error in the determination of ϵ is estimated to be 32% (Oakey, 1982). The wind speeds in the Emerald Basin study were measured to $\pm 10\%$ (Elliott, 1981) and in the JASIN study to better than $\pm 5\%$ yielding a maximum relative error in U_{10}^3 of order 50% between the two experiments. Together, these errors do not account for the observed difference. It must be due to fundamental differences in the generation mechanisms at the two sites.

The dissipation level at the same wind speed is found to decrease with depth as shown in Fig. 4. For each of three depth intervals: (A) 4–20 m, (B) 20–37 m, and (C) 37–56 m the average value of dissipation, $\bar{\epsilon}(z)$, was computed from 4 to 6 realizations at each station. The dependence on U_{10}^3 is evident in all three depth intervals above $U_{10}^3 \approx 100$ m^3 s^{-3} (a wind speed of 4.6 m s^{-1}); below this speed the dependence is not so obvious. From the lines drawn through the three sets of data, the dissipation at $U_{10}^3 = 1000$ is: Block A with a mean depth of 12 m, $\epsilon = 2 \times 10^{-7}$ m^2 s^{-3}; Block B with a mean depth of 28 m, $\epsilon = 4 \times 10^{-8}$ m^2 s^{-3}; and Block C with a mean depth of 46 m, $\epsilon = 2 \times 10^{-8}$ m^2 s^{-3}. If the dissipation per unit mass for the JASIN data decreases with depth as a power law z^{-M} the results from Fig. 4 indicate that $1 \leqslant M \leqslant 2$. For the discussion to follow we will consider a simple inverse depth dependence with $\bar{\epsilon} \alpha z^{-1}$. This dependence was found by Dillon *et al.* (1981) in studies in a lake. Because of the dependence of ϵ on surface energy input (parameterized by U_{10}^3) it is convenient to form the dimensionless quantity $\bar{\epsilon} z / U_{10}^3$ and examine differences in this quantity between sites.

This dissipation quantity may depend on the stratification which is conveniently parameterized in terms of the Brunt-Väisälä, frequency;

$$N = \left[\frac{-g}{\rho} \frac{\partial \sigma_t}{\partial z} \right]^{1/2} \quad [\text{s}^{-1}]. \tag{5.1}$$

Average values of N (converted to cycles/hour) for each block of microstructure data were obtained from CTD profiles obtained just before or just after each microstructure station for both the Emerald Basin and JASIN data sets. To examine the dependence on stratification, $\bar{\epsilon} z / U_{10}^3$ data were grouped in bands of constant $\log(N)$ and averaged. The data are plotted in Fig. 5. There is a tendency for $\bar{\epsilon} z / U_{10}^3$ to decrease with increasing density gradient (larger N) but the trend is not well defined. In Fig. 5 the dashed line defines a dependence of $\bar{\epsilon} z / U_{10}^3$ on N to the power $N^{-1/2}$. This is consistent with the JASIN data, but equally well, no dependence on N could be argued, particularly for the Emerald Basin data.

An estimate of the quantity $\epsilon z / U_{10}^3$ may be made if the mixing layer can be assumed to be a constant-stress boundary layer (e.g., see Turner, 1973). The shear for such a layer is given by

$$\frac{\partial U}{\partial z} = \frac{u_*}{kz} \tag{5.2}$$

where u_* is the friction velocity defined by

$$u_*^2 = \frac{\rho_a}{\rho_w} C_D U_{10}^2 \tag{5.3}$$

and $k = 0.4$ is Von Karman's constant, ρ_a and ρ_w are the density of air and water, respectively, and C_D is the drag coefficient. If production and dissipation are in balance (Eq. 1.1) then

$$\epsilon = \frac{u_*^3}{kz} = \left(\frac{\rho_a}{\rho_w} C_D \right)^{3/2} \frac{U_{10}^3}{kz}. \tag{5.4}$$

Equivalently,

$$\frac{\epsilon z}{U_{10}^3} = \left(\frac{\rho_a}{\rho_w} C_D \right)^{3/2} \frac{1}{k}$$

$$= \left\{ \frac{1.2 \text{ kg m}^{-3} \times 1.3 \times 10^{-3}}{10^3 \text{ kg m}^{-3}} \right\}^{3/2} \frac{1}{0.4} = 4.9 \times 10^{-9}.$$

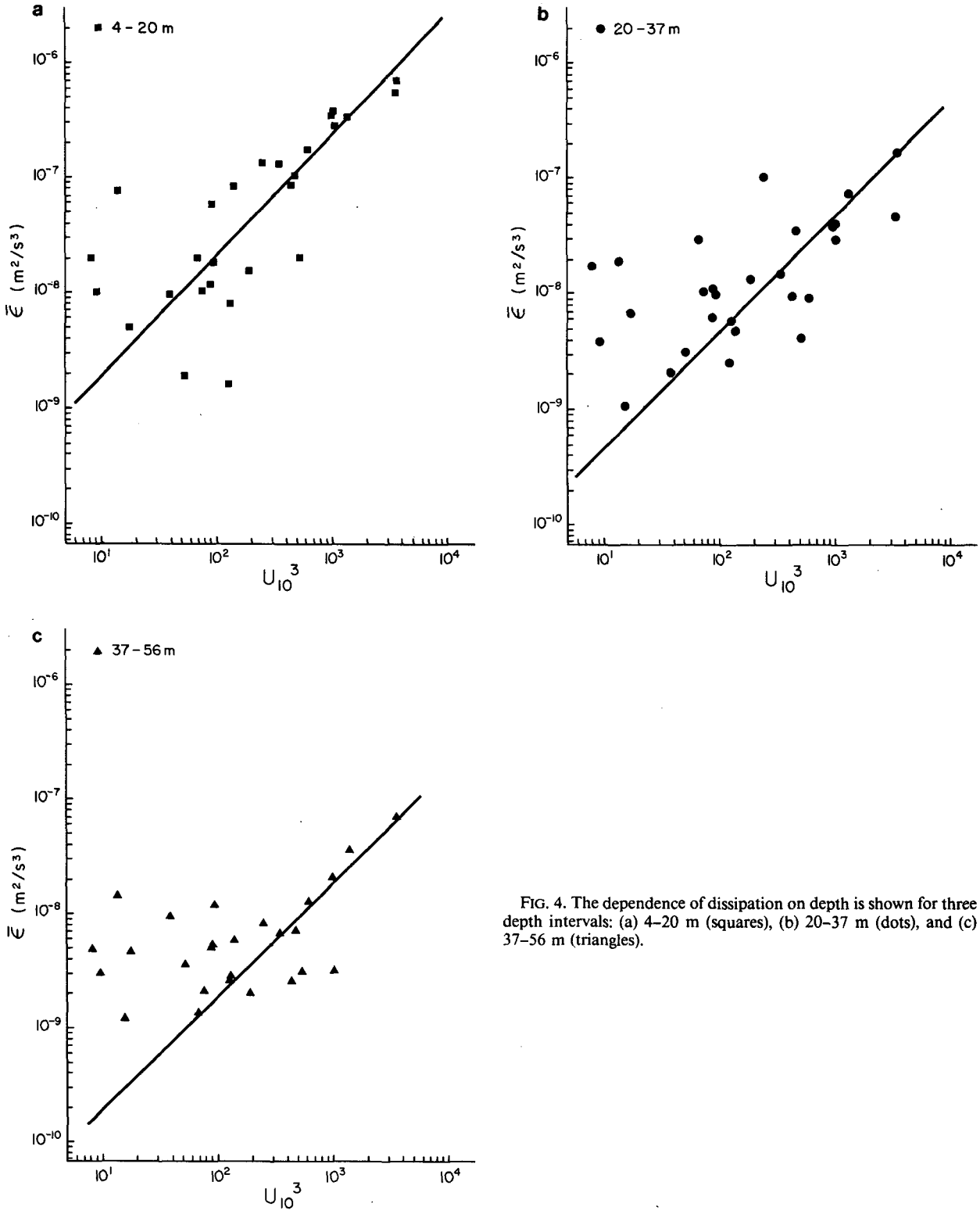

FIG. 4. The dependence of dissipation on depth is shown for three depth intervals: (a) 4–20 m (squares), (b) 20–37 m (dots), and (c) 37–56 m (triangles).

Thus, using the constant-stress boundary layer model, the constant derived assuming no stratification is in remarkable agreement with the experimental data as indicated by the horizontal line in Fig. 5. As pointed out in the Introduction (Eq. 1.1), even the simplified balance equation includes the buoyancy term, the en-

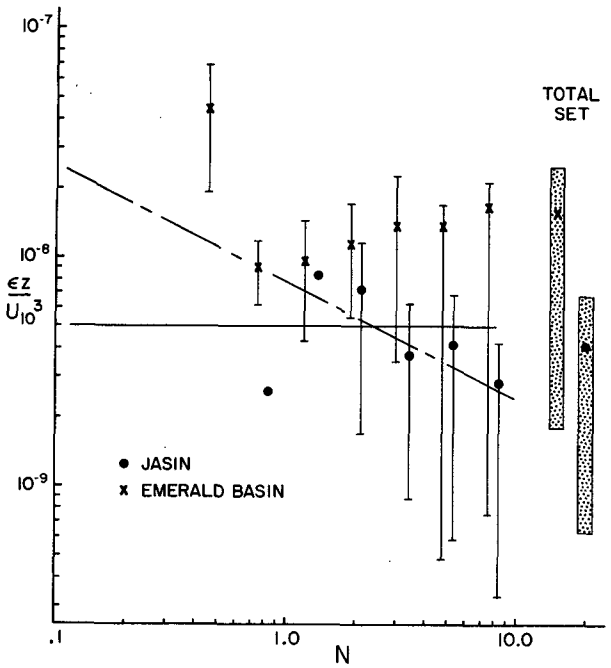

FIG. 5. The data $\epsilon z/U_{10}^3$, grouped in constant $\log_{10}N$ bands, are plotted versus the buoyancy frequency, N (cycles/hour), for the JASIN experiment (dots) and the Emerald Basin experiment (crosses).

ergy used in work against buoyancy forces to change the potential energy of the system, although as shown later, this term is only $\approx 20\%$ ϵ. Dillon *et al.* (1981) found agreement with a constant stress layer in a wind driven mixed layer in a lake. The present results imply that as a first approximation this may also be used in describing the oceanic boundary layer.

The constant-stress boundary layer arguments yield a value that is more consistent with the JASIN results than those from Emerald Basin, which have higher values of $\bar{\epsilon}z/U_{10}^3$. It may well be that the source of turbulence in the JASIN experiment was primarily from surface forcing. In contrast, the Emerald Basin experiment may have had a strong additional generation source from mean shears originating in the inertial period oscillations.

In the Emerald Basin study, a mooring was placed with a current meter in the mixed layer at a depth of 12 m and a second meter at 46 m. The predominant currents were at near-inertial frequency with a difference of 0.3 to 0.4 m s^{-1} between the two meters (Fig. 4, Oakey and Elliott, 1982). Measurements with a profiling current meter in that experiment indicated that the inertial shear and the mean density gradient resulted in relatively small gradient Richardson numbers both in the mixed layer and at its base. It was speculated that the link between mixed layer turbulence and the surface wind field may be not only from generation at near surface from processes such as wave breaking but as well may be a result of instabilities caused by near-inertial shears.

During JASIN, there were many current meter moorings, in particular those reported by Weller (1982) for moorings W2 (59°01′N, 12°33′W) and H2 (59°25′N, 12°30′W). These two sites are in the vicinity of the majority of the microstructure observations. He found large differences in the amplitude of inertial oscillations between the two sites. Therefore for purposes of comparison to microstructure observations in the larger area shown in Fig. 1 his results may not be entirely appropriate. Referring to Weller's Fig. 10, the magnitude of the inertial oscillations at W2 from 20 August to 2 September was about 5–10 cm s^{-1} and at H2 was 10–15 cm s^{-1} over the same period. The mixed layer tended to move as a slab with the inertial wave magnitude reduced by an order of magnitude below. This differed from the Emerald Basin area where the amplitude of the inertial period oscillations below the mixed layer was about half that in the mixed layer but shifted in phase resulting in large 0.3 to 0.4 m s^{-1} velocity differences. Since the density gradient in both experiments was similar, this factor of 2 in the velocity shear would result in average gradient Richardson numbers about 4 times as large in the JASIN experiment. Consequently, the tendency for production of turbulence from this source would be smaller in the JASIN study.

5. Temperature microstructure and related quantities

Temperature microstructure is produced in the mixing process by the straining of the temperature field by shears associated with the turbulent velocity field. This is expressed simply in Eq. (1.3), which in steady state expresses the equality of production of temperature variance by the turbulent field and the mean gradient balanced by the removal of temperature variance by molecular diffusion, χ_T. Measured values of χ_T during JASIN are shown in Fig. 2. They vary from the noise level of 1×10^{-8} °C^2 s^{-1} to as large as 2.7×10^{-6} °C^2 s^{-1} on day 248 just below the base of the mixed layer after a day of freshening winds.

Because the production of temperature variance and hence χ_T in the simple balance is dependent on the intensity of turbulence, we might expect that χ_T will show a dependence on the surface stress or U_{10}^3. An examination of the data indicates that indeed there is a tendency for χ_T to increase with increasing wind speed, though not as markedly as for ϵ. Of course it is well known that production of temperature variance depends on the mean gradient as well. The Cox number, which is the ratio of the temperature gradient variance (or χ_T) to the square of the mean temperature gradient, is a better quantity to compare with the surface stress than χ_T because it has the dependence on the mean gradient (which may vary spatially independent of the wind speed) removed. The Cox number is plotted versus U_{10}^3 in Fig. 6. Each point plotted is the average of 4–6 profiles within the depth intervals A, B

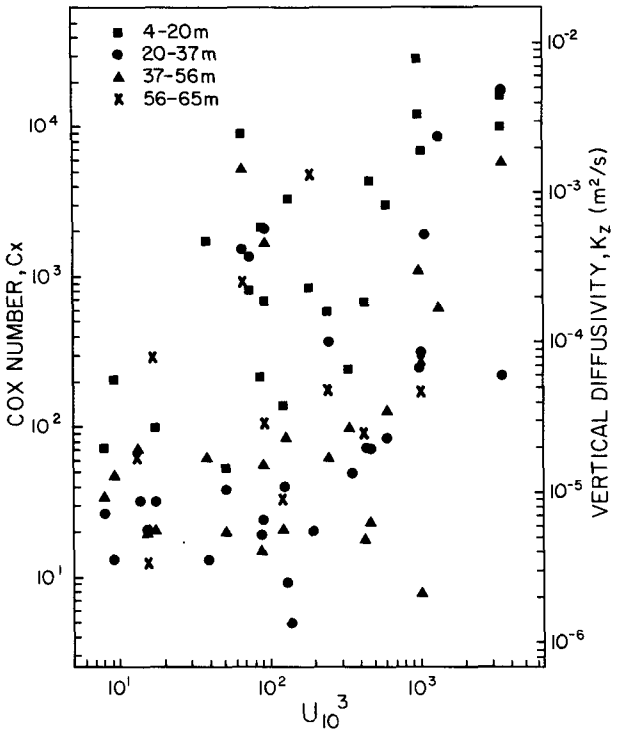

FIG. 6. The Cox Number, C_x, is plotted versus U_{10}^3 for four depth intervals. At the right, the axis for vertical diffusivity corresponding to the Cox Number data is shown.

and C defined previously and a deeper interval D (56–65 m). Directly related to the Cox number is the vertical eddy diffusivity, K_T, given by Eq. (1.6). The scale for $K_T = 2DC_x$ (where $D = 1.39 \times 10^{-7}$ m^2 s^{-1} is the thermal diffusivity) is plotted as the right hand ordinate of Fig. 6. It is evident that there is a strong dependence of C_x (or K_T) on U_{10}^3 as there was for ϵ. In particular this is true for Block A (4–20 m). The values tend to decrease with depth and Blocks C and D indicate a dependence on U_{10}^3 only for U_{10}^3 greater than 100 m^3 s^{-3} as was the case for ϵ in Fig. 4c.

Another quantity derived from the temperature gradient variance and the mean temperature gradient is the vertical heat flux, Q (W m^{-2}) given by Eq. (1.7). In the JASIN experiment, the mixing layer was on average warmer than below so the computed values of Q represent a positive heat flux downwards. The data of the Blocks A through D have been averaged to obtain a mean value for vertical heat flux, $\bar{Q}$, which may be compared to estimates made by others during the experiment. Values of $\bar{Q}$ obtained from the microstructure measurements are plotted in Fig. 7 versus U_{10}^3 and like C_x show an increase as the surface stress increases. In the JASIN experiment, the surface heat flux was measured by Guymer *et al.* (1983). They measured the radiative, sensible, and latent heat flux and computed the heat flux into the ocean. They estimate a mean value of 47 W m^{-2} over the period of 22 August to 4 September (day 234–247). From the CTD results of Prangsma *et al.* (1983) (e.g., their Fig. 4) one obtains a value of 39 W m^{-2} for the period of 22 August to 22 September. The two sets of measurements, surface heat flux and heat content of the water from CTDs are considered to be in agreement. From the average value of U_{10}^3 of $\approx$550 m^3 s^{-3} and the relationship of $\bar{Q}$ versus U_{10}^3 in Fig. 7, the microstructure measurements indicate a value of 20 W m^{-2}. This is lower than the values above, but, considering the errors associated with each measurement, is not inconsistent.

6. Mixing efficiency

The quantity, Γ, given by Eq. (1.10) has been derived by assuming that the vertical diffusivities for heat and mass are the same. The temperature gradient and its variance give a measure of the potential energy increase during mixing. The dissipation, ϵ, gives a measure of the kinetic energy dissipated in mixing. The quantity, Γ, is then a ratio of the change in potential energy to the change in kinetic energy, ΔPE/ΔKE, and may therefore be thought of as a "mixing efficiency." Because it is computed from fluctuating quantities, it may not represent the energy partition in the final mixed state.

Equation 1.10 is examined in Fig. 8 showing plots of ϵ versus $\chi_T/(\partial T/\partial z)$ for all of the blocks of data for which $\epsilon > 10^{-9}$ m^2 s^{-3} ($\epsilon_{noise} = 2 \times 10^{-10}$ m^2 s^{-3}) and for $\chi_T > 5 \times 10^{-8}$ °C^2 s^{-1} ($\chi_{T\,noise} = 2 \times 10^{-8}$ °C^2 s^{-1}). These criteria were selected to exclude poorly resolved data from the calculation of Γ. There were approximately 275 values of Γ satisfying these criteria for 10–15 m blocks of data for all depths. Lines of constant Γ are calculated using equation (1.10) with the isotropy factor equal to ⅓. Values in Fig. 8 are scattered from 0.01 to 1.0 grouped around a mean value of 0.25. In Blocks A (4–20 m) and B (20–37 m), the data from the mixed layer, points are quite scattered. Deeper than

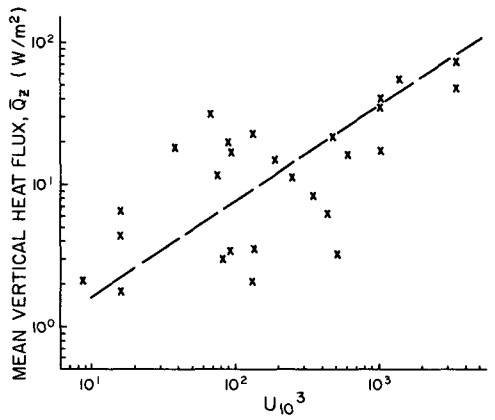

FIG. 7. The mean vertical heat flux averaged over depth to 60 m is plotted versus U_{10}^3.

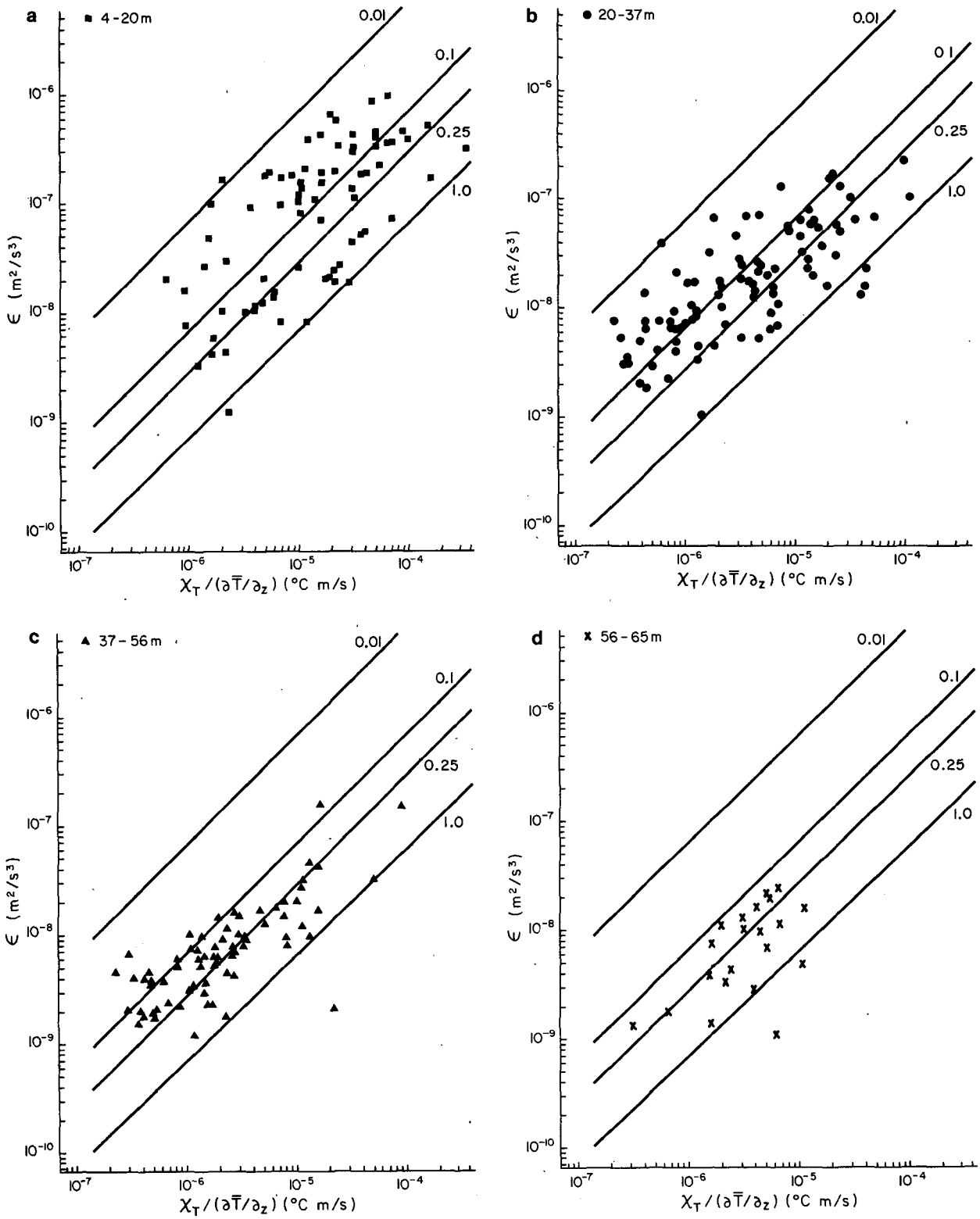

FIG. 8. Plot of ϵ vs $\chi_T/(\partial T/\partial z)$ in four plots A through D corresponding to depth intervals A, B, C, D described in the text. The lines represent values of constant mixing efficiency, Γ.

this in Blocks C (37–56 m) and D (56–65 m) the values cluster more closely to the value 0.25.

The distribution of Γ was examined as follows. The data were grouped in 20 bands of constant $\log_{10}(\Gamma)$ from $\Gamma = 0.01$ to $\Gamma = 1.0$ and arbitrarily into two bands of buoyancy frequency N, one for $0 < N < 4$ cycles/hour and a second for $4 < N < 10$ cycles/hour to distinguish weaker and stronger stratification respectively. The histograms of the data grouped in this way are shown in Fig. 9. Although there are fewer values of Γ for $0 < N < 4$ cycles/hour they are more clearly spread out in Γ with no clearly defined peak. Values of Γ for $4 < N < 10$ cycles/hour are less spread out and show a well defined peak at $\Gamma = 0.25$. This grouping for weaker stratification includes most of the upper-layer data which are those for which the wind forcing generates more turbulence and ϵ is higher.

The apparent difference in the distribution of Γ values for lower and higher N values may be an indication of different dynamics (because of the differing importance of buoyancy forces) in these regimes. The small number of points, however, makes this interpretation very speculative. For this reason, the values of Γ have been considered as one set. Assuming that the set is a lognormal distribution (discussed later) the mean value of Γ is found to be $\bar{\Gamma} = 0.265$. The 1σ confidence intervals (from the lognormal distribution) then define $0.066 < \Gamma < 0.436$. This mixing efficiency, $\bar{\Gamma} = 0.265$, corresponds to a flux Richardson number,

$$R_F = \Gamma/(1 + \Gamma) = 0.21.$$

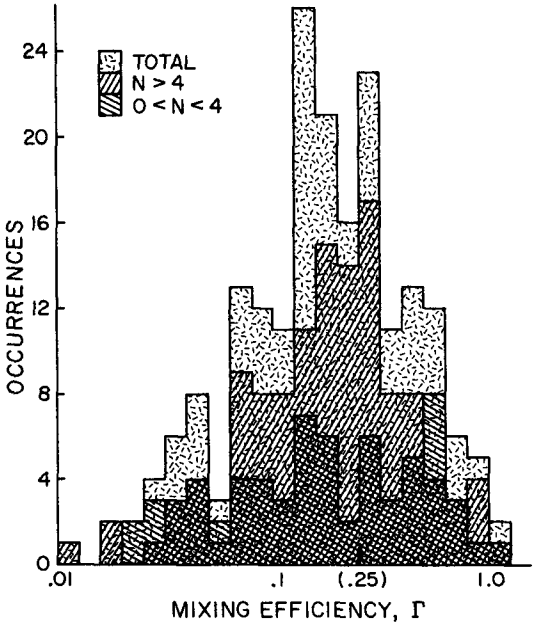

FIG. 9. The mixing efficiency, Γ, is plotted as a histogram for two ranges of buoyancy frequency, N: $0 < N < 4$ cycles/hour and $4 < N < 10$ cycles/hour.

The flux Richardson number is the ratio of buoyancy production to turbulent kinetic energy production (the ratio of the third to first term on the right of Eq. 1.1). In steady state R_f must be less than 1 and it has been argued that it must be much less than 1. Stewart (1959) argued that the energy loss to buoyancy is only affected by $\bar{w}^2$ whereas loss to viscosity affects three components $\bar{u}^2$, $\bar{v}^2$ and $\bar{w}^2$. Since the pressure fluctuation mechanism that transfers energy from one velocity component to another is likely much less efficient than the decay mechanism, R_f must be appreciably less than unity. Ellison (1957) proposed theoretically a critical flux Richardson number $R_{f\,\mathrm{crit}} = 0.15$ based on the equations of turbulent energy, mean-square temperature fluctuations and turbulent heat flux and the implied behavior of α, the ratio of diffusion coefficients for heat and momentum. Arya (1972) disputed these assumptions about α and proposed that the critical condition arises from maintaining an equilibrium shear stress. Based on the equations of Reynolds stress and turbulent energy an expression for $R_{f\,\mathrm{crit}}$ in terms of correlation and anisotropy coefficients was estimated to be $R_{f\,\mathrm{crit}} = 0.15$ to 0.25. Weinstock (1978) derived the constant $\Gamma = 0.81$ theoretically by considering only the scales within the inertial subrange. The corresponding value for R_f is 0.45, much larger than previous estimates.

The present set of oceanic results indicates a value of $R_f = 0.21$ in good agreement with the estimates of Arya (1972). They are also in agreement with Britter's (1974) laboratory results, which suggest a critical flux Richardson number of 0.18 to 0.20.

7. Statistics of microstructure fluctuations

One of the characteristic features of turbulence displayed by the measurement of oceanic microstructure is the extreme variability in space and time. In vertical profiles, the observed patches of structure of order meters thick may vary in intensity by orders of magnitude with depth. A subsequent profile observed just a few minutes later may bear little resemblance to the original. The statistical variability of quantities like dissipation has been discussed by Gurvich and Yaglom (1967). Their paper presents a theoretical treatment leading to the prediction that certain quantities, such as the dissipation rate, should have lognormal probability distributions. The assumptions apply to isotropic, homogeneous high Reynolds number turbulence at typical length scales greater than the viscous cut-off scale and less than the scales of the energy containing eddies. In the present analysis, the data have been considered in vertical blocks of 10–15 m and there is no *a priori* reason to expect that these results will be lognormally distributed. It is assumed that this distribution is appropriate in an effort to understand the errors associated with mean quantities such as $\epsilon(z)$. It is through comparison of mean quantities averaged over a suitable spatial and temporal scale that one relates dissipation

and other microstructure quantities to large-scale forcing such as the surface stress in the mixed layer or to shear production by inertial period oscillations. The data are not normally distributed and, as shown below, microstructure quantities measured in this experiment may be described statistically with a lognormal distribution.

Lognormal distributions have been well studied, and are described by Aitchison and Brown (1969) and Hald (1952). Following Hald (1952), a lognormal distribution of a variate x is one where $y = \log x$ is distributed according to a normal law. Therefore mean $(\log x_i) = \log\zeta$ and variance $(\log x_i) = \sigma^2$. From this the mean of the x distribution is mean $(x) = \zeta \times 10^{\sigma^2/2M}$ where $M = \log e$. As well, median $(x) = \zeta$ and mode $(x) = \zeta \times 10^{\sigma^2/M}$. The 95% confidence intervals are given by $\zeta/(10^{1.96\sigma}) <$ mean $(x) < \zeta \times 10^{1.96\sigma}$, and the 68% confidence intervals by $\zeta/(10^{0.98\sigma} <$ mean $(x) < \zeta \times 10^{0.98\sigma}$. For temperature microstructure, Elliott and Oakey (1979) found that the Cox numbers in the equatorial pycnoclines were distributed lognormally and Crawford (1982) found a similar distribution for measurements of dissipation in the Equatorial Pacific.

The short-term variability in dissipation, $\epsilon(z)$, is illustrated in Fig. 10. Each point was obtained by dividing each $\epsilon(z)$ by the mean of 4–6 values at that 10–15 m depth interval, $\bar{\epsilon}(z)$. These data were grouped into bands of constant $\log[\epsilon(z)/\bar{\epsilon}(z)]$ and are plotted as a histogram in Fig. 11. The cumulative probability plot for this histogram, in Fig. 12, indicates that the distribution deviates somewhat from lognormality, in particular in the excess of small values, which may be contributed partly to improperly subtracting noise in the low signal-to-noise sections of the data. A chi-squared goodness-of-fit test indicates that although the fit to the lognormal distribution is poor, the hypothesis cannot be rejected. For the best-fit lognormal curve the mean $(\log\epsilon/\bar{\epsilon}) = -0.04$ [mean $(\epsilon/\bar{\epsilon}) = 1.2$] and the standard deviation is 0.32. Thus 68% of the data lie between the limits 0.43 < mean $(\epsilon/\bar{\epsilon}) < 1.91$. Because the mean dissipation, $\bar{\epsilon}$, is a quantity used in models, it is instructive in planning an experiment to ask how well the mean is estimated by n observations. Because the standard deviation of the mean depends on $\sqrt{n}$ the limits are defined by

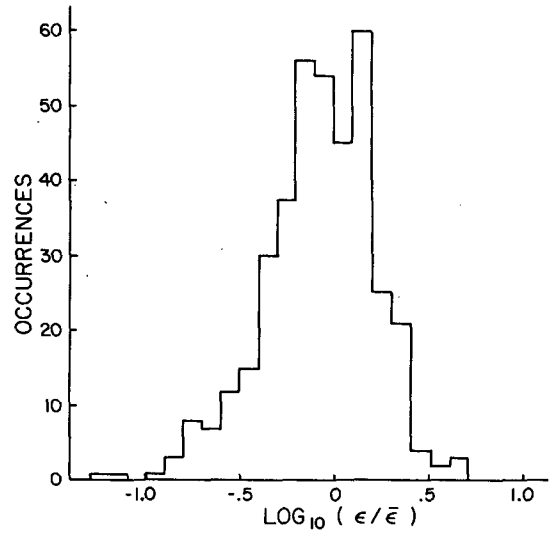

FIG. 11. The histogram of values of $\epsilon/\bar{\epsilon}$ shown in Fig. 10.

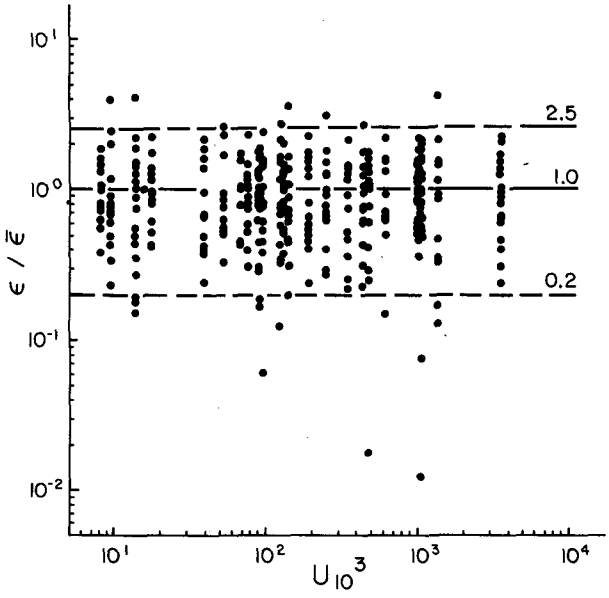

FIG. 10. Individual values of dissipation, $\epsilon(z)$, divided by the station mean, $\bar{\epsilon}(z)$, are plotted versus U_{10}^3.

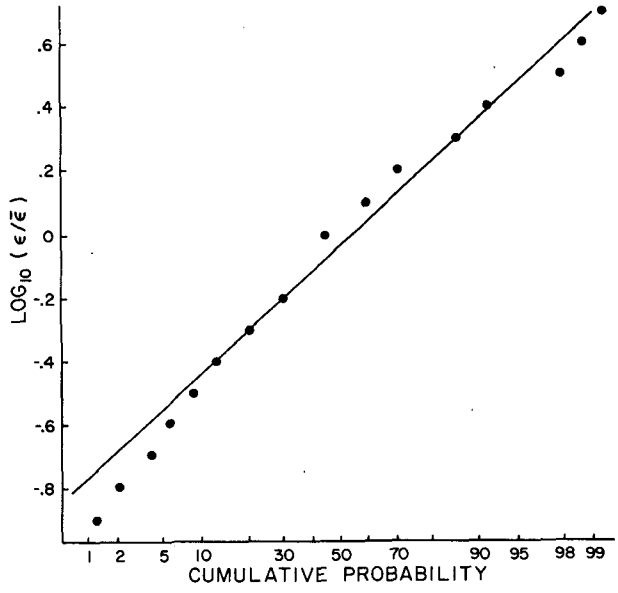

FIG. 12. The cumulative probability plot of the data of the histogram of Fig. 11 is plotted to show the lognormal dependence.

$$\zeta/10^{0.98\sigma/\sqrt{n}} < \text{mean } (x) < \zeta \times 10^{0.98\sigma/\sqrt{n}}.$$

For the above example, where $\sigma = 0.32$ one requires at least 16 realizations to achieve 20% precision in $\bar{\epsilon}$. For the present experiment with five realizations per station over a period of 25 minutes, the standard deviation in $\bar{\epsilon}$ is about 40%.

The dependence of $\bar{\epsilon}z/U_{10}^3$ on the density gradient (parameterized by the buoyancy frequency, N) was examined previously and the results plotted in Fig. 5. If one assumes there is no dependence on N and that the variability is statistical, are the distributions for the two experiments different? The histogram of data, $\bar{\epsilon}z/U_{10}^3$, is shown in Fig. 13 for both the JASIN and Emerald Basin studies. The corresponding cumulative probability plots are shown in Fig. 14. With the assumption that both sets are lognormal, the largest deviation is in the excess of low values for the Emerald Basin data. The standard deviations for the JASIN and Emerald Basin experiments of 0.55 and 0.40 respectively, indicate that the JASIN results are much more scattered. The value of 0.55 for the JASIN data is larger than $\sigma = 0.28$ for the $\bar{\epsilon}/\epsilon$ data reflecting the additional variability of the mean $\bar{\epsilon}$ (presumably spatial and temporal effects) even though the predominant forcing parameters, depth and surface stress have been normalized in the $\epsilon z/U_{10}^3$ distribution. The standard deviation of the mean for the Emerald Basin set (52 pts) is ±13% and for the JASIN set (44 points) is ±20% using the values of $\sigma = 0.40$ and 0.55 respectively. The ratio of the means for the two sets is ≈ 3 so there is little doubt that the distributions for the two sets are different and there is much more velocity microstructure at a given wind speed during the shelf experiment as compared to JASIN.

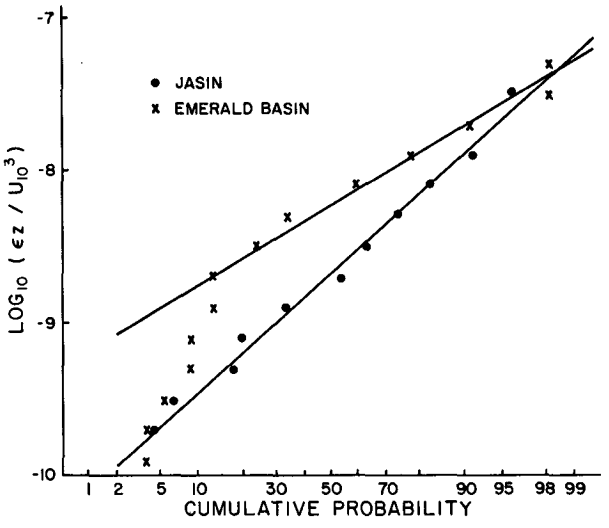

FIG. 14. Cumulative probability distributions of $\log(\bar{\epsilon}z/U_{10}^3)$ for the JASIN and Emerald Basin data are plotted to show lognormal dependence.

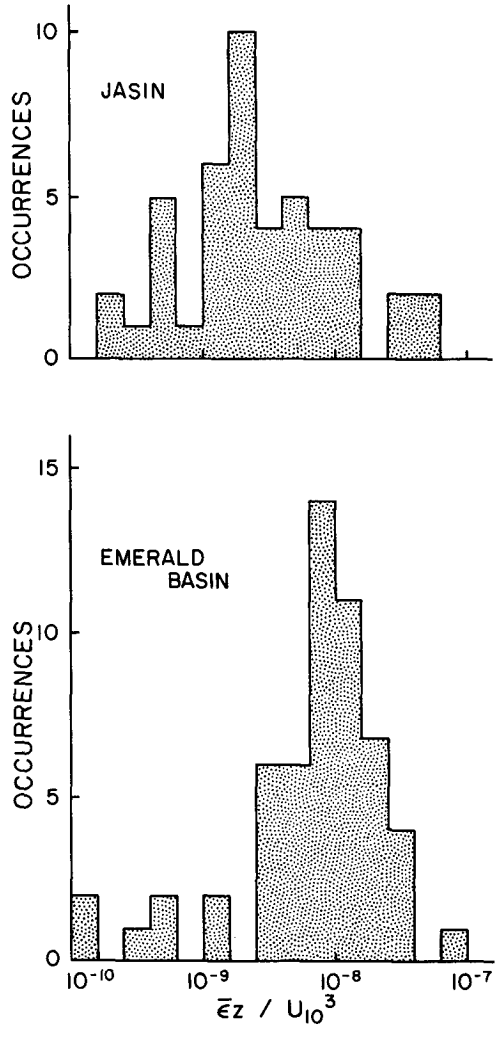

FIG. 13. The histogram of $\bar{\epsilon}z/U_{10}^3$ for JASIN and Emerald Basin studies are shown.

As outlined by Aitchison and Brown (1969) a product (or ratio) of two independent lognormally distributed variates is also a lognormally distributed variate. The mixing parameter, Γ, is the ratio of $\chi_T/(\partial T/\partial z)$ and ϵ. The normalized dissipation was described above as a lognormal distribution and, although not shown in this paper, the temperature gradient factor may also be described with this distribution. The temperature Cox number has been shown to be lognormally distributed by Elliott and Oakey (1979). The mixing parameter might reasonably be then described as a lognormal distribution and has been displayed as such by plotting Γ grouped into constant $\log(\Gamma)$ bins as a histogram in Fig. 9. The cumulative probability for the whole set of data is shown in Fig. 15 where the best-fit lognormal line is shown superimposed on the data. The data indicate a mean(Γ) = 0.265 with one standard deviation confidence intervals as $0.066 < \text{mean } (\Gamma) < 0.436$ ($\log\zeta = 0.76$ and $\sigma = 0.42$).

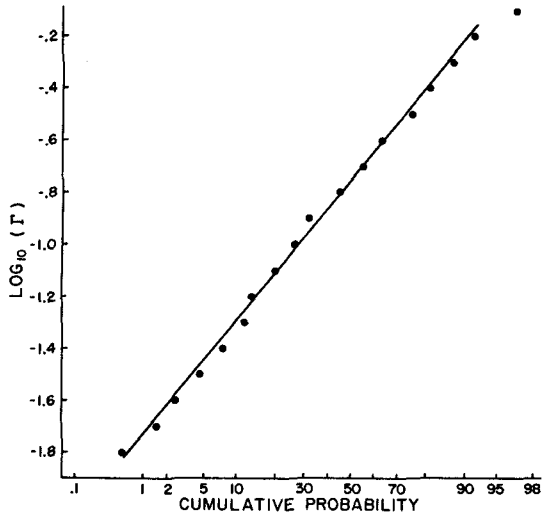

FIG. 15. Cumulative probability distribution of $\log_{10}\Gamma$ is plotted to show lognormal dependence.

8. Discussion and conclusions

The simultaneous measurements of velocity and temperature microstructure in the upper 70 m during JASIN have been used to estimate turbulent energy dissipation, ϵ, and the dissipation of temperature fluctuations, χ_T. Both of these quantities, and their relationship to one another and to the large-scale (temporal and spatial), are important links in our understanding of mixing processes in the upper layers of the ocean in response to forcing such as the surface wind stress. The dissipation is found to depend linearly on the cube of surface wind speed U_{10}^3 particularly for $U_{10}^3 > 100$ m^3 s^{-3}. Two experiments, one on the Scotian shelf (Emerald Basin) and the second in the JASIN study, however, give different constants of proportionality. The Emerald Basin study indicated that at least 1.2% of the energy flux from the atmospheric boundary layer appeared as dissipation in the mixed layer while the JASIN study indicated only 0.4%. Comparison to studies of Denman and Miyake (1973) shows that dissipation represents a much larger fraction of the energy than that producing mixed layer deepening (0.12%). The differences between the shelf experiment and the JASIN study are open questions. There were similar density gradients (or buoyancy frequencies) in both studies. In the shelf study there appeared to be much larger near-inertial currents concentrated near the base of the mixing layer than in JASIN, which could generate turbulence through low Richardson number instability. Since the intensity of near-inertial currents depends upon the wind speed as well, both sets of data could show the dependence on U_{10}^3 whether turbulence were generated from the surface downwards or by inertial shears in the mixing layer. If one assumes there is a constant-stress boundary layer, one finds that the expected dissipation rate is consistent with those measured during JASIN and lower than those measured during the Emerald Basin study as indicated in Fig. 5. Although the assumption of a constant stress layer is weak, the results strengthen the argument for additional sources of turbulent generation rather than surface stress in the Emerald Basin study.

The measurement of temperature microstructure allows one to calculate a vertical heat flux, Q, (Eq. 1.7) which, as shown in Fig. 7, increases as U_{10}^3 increases. A comparison of Q from microstructure studies ($\approx$20 W m^{-2}) indicates a value about half that determined from the large scale JASIN studies of Guymer *et al.* (1983) (47 W m^{-2}) and Prangsma *et al.* (1983) (39 W m^{-2}). Although the errors associated with each measurement make these consistent, one might expect the measured turbulent heat flux to be smaller than the total. Because the microstructure measurements are an average over the upper 60 m and the heat flux decreases with depth, the estimate of 20 W m^{-2} should be lower than the surface heat flux. Radiative heating decreasing with depth, longwave radiation, evaporation and conductive cooling at the surface all contribute to the vertical heat flux. The entire net heat flux across the sea surface need not be carried by turbulence. The turbulent heat flux measurement represents heat given up or absorbed by parcels of water displaced from their equilibrium position in the water column by turbulence. The results indicate that at least half the heat flux may be carried by turbulent processes.

Simultaneous measurements of ϵ and χ_T have been used to calculate a mixing efficiency, Γ, the ratio of the increase in potential energy in the mixing process to the loss of turbulent kinetic energy. The Γ is distributed lognormally and has, in this experiment, values from 0.01 to 1 with mean $(\Gamma) = 0.265$ with 68% of the values between 0.066 and 0.436. The mean value of Γ corresponds to a flux Richardson number $R_f = 0.21$ which is consistent with theoretical arguments and laboratory measurements of a critical flux Richardson number of 0.18 to 0.20 (Britter, 1974). As discussed by Osborn (1980), the vertical diffusivity may be estimated from Eq. (1.9) using the notion of a critical flux Richardson number to estimate Γ. The present set of data indicates that Γ has a wide range of values which are presumably related to the natural variability in the mixing process and not statistical errors. Random errors of measurements should result in a distribution which is normal, not lognormal. One must therefore be cautious in using Eq. (1.9) to calculate $K\rho$ because of the variability in the parameter, Γ.

An alternative way of interpreting Figs. 8a–8d is that they are plots of a variable proportional to $K\rho$ (ordinate) versus a variable proportional to K_z (abscissa). The ratio $K\rho/K_z$ given using Eqs. (1.4), (1.6) and (1.9) is

$$\frac{K\rho}{K_z} = \frac{(\Gamma/g\alpha)\epsilon}{(1/3 \pm 1/6)\chi_T/(\partial\bar{T}/\partial z)}; \qquad (8.1)$$

so the axes would require scaling to give the correct units. As indicated by the confidence intervals for Γ, the two estimates of vertical diffusivity are the same only within an order of magnitude using a constant value for Γ.

The lognormal distribution of microstructure quantities seriously limits the accuracy of a measurement of a mean quantity such as $\bar{\epsilon}$ for use in a simple balance equation such as Eq. (1.1). For example, the standard deviation for $\epsilon z/U_{10}^3$, a dimensionless dissipation quantity in which the major forcing and depth dependence has been removed is $\sigma = 0.55$. This implies that the order of 50 observations would be required to obtain an estimate of the mean with an uncertainty of $\pm 20\%$.

Acknowledgments. I would like to thank J. Elliott and Peter Pozdnekoff who, along with the author, collected the microstructure data from the RRS *Shackleton* during the JASIN experiment. I would also like to thank the JASIN experiment organizers and, in particular, R. Pollard for their encouragement and assistance in our participation in the experiment.

REFERENCES

Aitchison, J., and J. A. C. Brown, 1969: *The Lognormal distribution,* Cambridge University Press, 176 pp.

Arya, S. P. S., 1972: The critical condition for the maintenance of turbulence in stratified flows. *Quart. J. Roy. Meteor. Soc.,* **98,** 264–273.

Batchelor, G. K., 1959: Small-scale variation in convected quantities like temperature in a turbulent fluid. *J. Fluid Mech.,* **5,** 113–133.

Britter, R. E., 1974: An experiment on turbulence in a density stratified fluid. Ph.D. thesis, Monash University, Victoria, Australia.

Caldwell, D. R., 1983: Small-scale physics of the ocean. *Rev. Geophys. Space Phys.,* **21,** 1192–1205.

Crawford, W. R., 1982: Pacific equatorial turbulence. *J. Phys. Oceanogr.,* **12,** 1137–1149.

Denman, K. L., and M. Miyake, 1973: Upper layer modification at ocean station Papa: Observations and simulation. *J. Phys. Oceanogr.,* **3,** 185–196.

Dillon, T. M., J. G. Richman, C. G. Hansen and M. D. Pearson, 1981: Near-surface turbulence measurements in a lake. *Nature,* **290,** 390–393.

Elliott, J. A., 1981: Anemometer blockage on CSS *Dawson,* Bedford Institute of Oceanography, Res. Note No. 1, May 1981 (unpublished) 14 pp.

——, and N. S. Oakey, 1979: Average microstructure levels and vertical diffusion for Phase III, GATE. *Deep-Sea Res.* (GATE Suppl. I), **26,** 279–294.

Ellison, T. H., 1957: Turbulent transport of heat and momentum from an infinite rough plane. *J. Fluid Mech.,* **2,** 456–466.

Gurvich, A. S., and A. M. Yaglom, 1967: Breakdown of eddies and probability distributions for small-scale turbulence: *Phys. Fluids* **10**(*Suppl.,* Part II), 559–565.

Guymer, T. H., J. A. Businger, K. B. Katsaros, W. J. Shaw, P. K. Taylor, W. G. Large and R. E. Payne, 1983: Transfer processes at the air–sea interface. *Phil. Trans. Roy. Soc. London,* **A308,** 253–273.

Hald, A., 1952: *Statistical Theory with Engineering Applications,* Wiley & Sons, 783 pp.

Munk, W. J., 1966: Abyssal recipes. *Deep-Sea Res.,* **13,** 707–780.

Oakey, N. S., 1977: An instrument to measure oceanic turbulence and microstructure. BIO Rep. BI-R-77-3, 52 pp.

——, 1982: Determination of the rate of dissipation of turbulent energy from simultaneous temperature and velocity shear microstructure measurements. *J. Phys. Oceanogr.,* **12,** 256–271.

——, and J. A. Elliott, 1982: Dissipation within the surface mixed layer. *J. Phys. Oceanogr.,* **12,** 171–185.

Osborn, T. R., 1980: Estimates of the local rate of vertical diffusion from dissipation measurements. *J. Phys. Oceanogr.,* **10,** 83–89.

——, and C. S. Cox, 1972: Oceanic finestructure. *Geophys. Fluid Dyn.,* **3,** 321–345.

——, and T. E. Siddon, 1973: Oceanic shear measurements using the airfoil probe. *Proc. Third Biennial Symp. on Turbulence in Liquids,* G. K. Patterson, and J. L. Zaken, Eds., University of Missouri-Rolla, 41–55.

——, and W. R. Crawford, 1980: An airfoil probe for measuring velocity fluctuations in the water. *Air–Sea Interaction: Instruments and Methods,* F. W. Dobson, L. Hasse and R. Davis, Eds., Plenum, 369–386.

Pollard, R. T., T. H. Guymer and P. K. Taylor, 1983: Summary of the JASIN 1978 field experiment. *Phil. Trans. Roy. Soc. London,* **A308,** 221–230.

Prangsma, G. J., T. H. Guymer, P. Kruseman, R. T. Pollard and R. A. Weller, 1983: The development of the temperature and salinity structure of the upper ocean over two months in an area 150 × 150 km. *Phil. Trans. Roy. Soc. London,* **A308,** 311–325.

Siddon, T. E., 1971: A miniature turbulence gauge utilizing aerodynamic lift. *Rev. Sci. Instrum.,* **42,** 653–656.

Stewart, R. W., 1959: The problem of diffusion in a stratified fluid. *Advances in Geophysics,* Vol. 6, Academic Press, 303–311.

Turner, J. S., 1973: *Buoyancy Effects in Fluids,* Cambridge University Press, 368 pp.

Weinstock, J., 1978: Vertical turbulent diffusion in a stably stratified fluid. *J. Atmos. Sci.,* **35,** 1022–1027.

Weller, R. A., 1982: The relation of near-inertial motions observed in the mixed-layer during the JASIN (1978) experiment to the local wind stress and the quasigeostrophic flow field. *J. Phys. Oceanogr.,* **12,** 1122–1136.